PROGRESS IN PHOTOVOLTAICS: RESEARCH AND APPLICATIONS
*Prog. Photovolt: Res. Appl.* 2011; **19**:134–140
Published online 14 May 2010 in Wiley Online Library (wileyonlinelibrary.com). DOI: 10.1002/pip.994

RESEARCH ARTICLE

# Optimization of anti-reflection moth-eye structures for use in crystalline silicon solar cells

Noboru Yamada[1]*, Oanh Ngo Kim[1], Toru Tokimitsu[2], Yusuke Nakai[2] and Hideki Masuda[3]

[1] Department of Mechanical Engineering, Nagaoka University of Technology, Nagaoka, Japan
[2] Mitsubishi Rayon Co. Ltd., Tokyo, Japan
[3] Department of Applied Chemistry, Tokyo Metropolitan University, Hachioji, Japan

## ABSTRACT

An anti-reflection (AR) moth-eye structure made of acrylic resin and deposited on a polyethylene terephthalate (PET) substrate was optimized in the wavelength range from 400 to 1170 nm; crystalline silicon (c-Si) solar cells function efficiently in this wavelength range. The rigorous coupled wave analysis (RCWA) method was used for optical simulation, and the Taguchi method was used for efficient optimization. The simulation results showed that the reflectance of the optimized structure over the above-mentioned wavelength range was less than 0.87% and that a minimal reflectance of 0.1% was observed at 400 nm. Experimental results showed that the reflectance of a fabricated moth-eye structure was less than 1.0% in the wavelength range and that a minimal reflectance of 0.55% was observed at 700 nm. A c-Si solar cell, which was enclosed in a polyvinyl butyral (PVB) layer of uniform thickness, was coated with the fabricated moth-eye film, and it was observed that the moth-eye film increased electric generation (EG) up to 15%, depending on the incident angle. Further, a daily increase in EG of up to 8.7% was estimated on a clear summer day in Japan when the moth-eye film was used. Copyright © 2010 John Wiley & Sons, Ltd.

**KEYWORDS**

anti-reflection; moth-eye; crystalline silicon solar cells; nanoinprinting

***Correspondence**

Noboru Yamada, Noboru Yamada, Department of Mechanical Engineering, Nagaoka University of Technology, Nagaoka, Japan.
E-mail: noboru@nagaokaut.ac.jp

Received 18 May 2009; Revised 24 December 2009

## 1. INTRODUCTION

Minimizing optical reflection, which has always been a major challenge, is very important in devices that use renewable energy. Photovoltaic (PV) solar cells are made of materials such as Si, InP, GaAs, etc. that have high refractive indices. More than 35% of the incident sunlight is lost by reflection when anti-reflection (AR) films are not used [1]. Each semiconductor material has an optimum solar spectrum range for maximum electricity production. Photon energy outside this range is wasted. The optimum solar spectrum of typical solar cells such as crystalline Si (c-Si) solar cells is in the range from 400 to 1170 nm. Thus, it is important to minimize reflection over this wavelength range.

Reflection can be reduced by using an AR film with a quarter-wavelength optical thickness and a refractive index of $n = \sqrt{n_1 n_2}$, where $n_1$ and $n_2$ are the refractive indices of the ambient and substrate, respectively. The principle process of achieving the necessary low refractive indices is always the same, i.e., mixing the substrate material with air on a sub-wavelength scale.

Surfaces coated with a moth-eye structure of sub-wavelength roughness are known to show superior AR properties. Such a surface was first discovered on the cornea of night-flying moths by Bernhard [2] in 1967. The eyes of this insect are covered with a regular array of conical protuberances (nipples) with a spacing ranging from 180 to 240 nm and height varying between 0 and 230 nm. The reflectance of their cornea was investigated in the wavelength range from 300 to 700 nm [3,4]. Stavenga *et al.* [4] investigated 19 butterfly species and showed that the nipple shape plays a rather insignificant role in the reduction of reflectance. They also proved that the nipple width plays a secondary role, whereas the nipple height is the crucial factor. Reflectance is reduced as the height increases.

The first artificial moth-eye structure/film was produced by recording the interference patterns of two coherent laser beams on a photoresist [3]. Currently, master structures with a surface area of 0.5 $m^2$ can be produced by a complex holographic optical process or plasma treatment [5,6].

In recent times, glass surfaces are gradually being replaced with plastic surfaces as sub-wavelength AR

structures, because plastics are lightweight, they can be mass produced, and they are cheaper than glass [6]. Acrylic resin which consists of polymethyl methacrylate (PMMA) is one of the suitable polymers. It offers excellent optical properties with high molding precision at low costs. Therefore, the moth-eye film made by plastics has a potential to be deposited on the top of glass or plastic encapsulation layer of solar cells.

In this paper, a nanoimprinting technique using anodic porous alumina molds [7] is employed to deposit a moth-eye structure made of acrylic resin on a polyethylene terephthalate (PET) substrate, as shown in Figure 1. Large area, low cost moth-eye films can be fabricated by this method. Improving the AR efficiency in the range of solar radiation is vital for PV applications. Hence, the aim of this study is to optimize the moth-eye structure for use in typical PV cells (i.e., c-Si cells) so that reflection and absorption can be minimized and transmission can be improved over a spectrum range that matches that of the PV cells. In addition, AR is obviously important in concentrating PV applications using lens and cover aperture glass.

In this study, first, the reflectance of a modeled moth-eye structure is parametrically simulated and the significance of certain dimensions of the nipple is clarified. Then, the moth-eye film, which is deposited on a c-Si cell surface, is optimized in order to achieve the maximum transmitted power (TP). The rigorous coupled wave analysis (RCWA) method is used to simulate electromagnetic wave propagation, and the Taguchi method is used for optimization. Further, electric generation (EG) of the c-Si solar cell with the moth-eye film is experimentally measured and compared with that of a conventional c-Si cell enclosed in a polyvinyl butyral (PVB) layer of uniform thickness. Finally, the daily increase in EG of the c-Si solar cell with the moth-eye film is estimated.

## 2. SIMULATION METHOD AND MODEL

The simulation is carried out by the RCWA method [8–11], which analyzes the reflectance and transmittance of an electromagnetic plane wave incident obliquely on a grating structure composed of materials with different indices. In the RCWA method, full vectorial Maxwell's equations can be solved based on the coupled mode theory.

The geometrical structure of the modeled moth-eye structure used for RCWA is shown in Figure 2. While the shape of structure in Figure 2(a) looks smooth, it is noted that the structure is actually broken into numerous simple building blocks (layers in the present case) with a vertically homogeneous region as shown in Figure 2(b). Hence, the RCWA method gives an approximate solution of the Maxwell's equation for complex three-dimensional structures. Here, Region I, II, and III corresponds to air, moth-eye layer, and base layer, respectively. The grating is periodic in two independent directions, $x$ and $y$. A linearly polarized electromagnetic wave is obliquely incident at an arbitrary incident angle $\theta$ and azimuth angle $\phi$. $\psi$ is the angle between the electric-field vector and the plane of incidence. The magnetic and electric fields, respectively, are perpendicular to the plane of incidence at $\psi = 0^\circ$ and $\psi = 90^\circ$. The horizontal arrangement of the nipple lattice is assumed to be hexagonal. $\Lambda_x$ and $\Lambda_y$ are the grating periods along the $x$ and $y$ axes, respectively. In addition, optical constants: refractive index and extinction coefficient of the material used for each layer must be given for RCWA calculation. Those values of acrylic resin, PET, and c-Si used in after-mentioned experiment were measured in advance and applied to the simulation. It should be noted that the absorbance of acrylic resin and PET is quite small and negligible across the wavelength investigated in this study. For example, 99.997% of incident light penetrates through the acrylic resin layer of 1 mm thick. Therefore, the absorbance of acrylic resin and PET do not influence to overall result of the present study.

## 3. SIMULATION RESULTS

First, using the simulation models shown in Figure 3(a) and (b), the reflectance of the moth-eye structure is parametrically computed by varying the dimensions of the nipple—height $H$, top width $TW$, and bottom width $BW$. Then, by using the model shown in Figure 3(c), the nipple

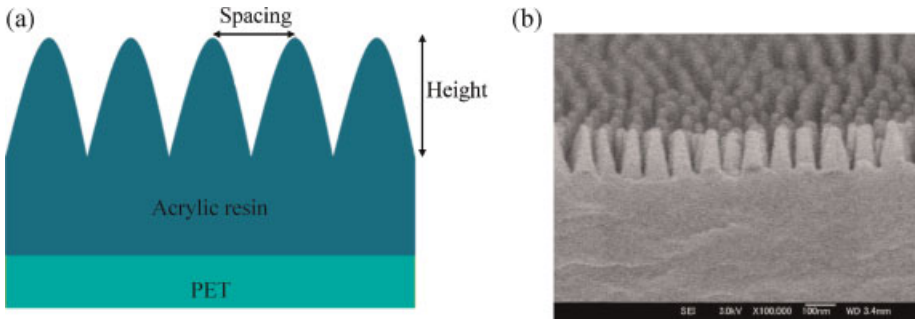


**Figure 1.** Moth-eye structure made of acrylic resin deposited on PET substrate. (a) Schematic of moth-eye structure. (b) Fabricated moth-eye structure, as observed using SEM.

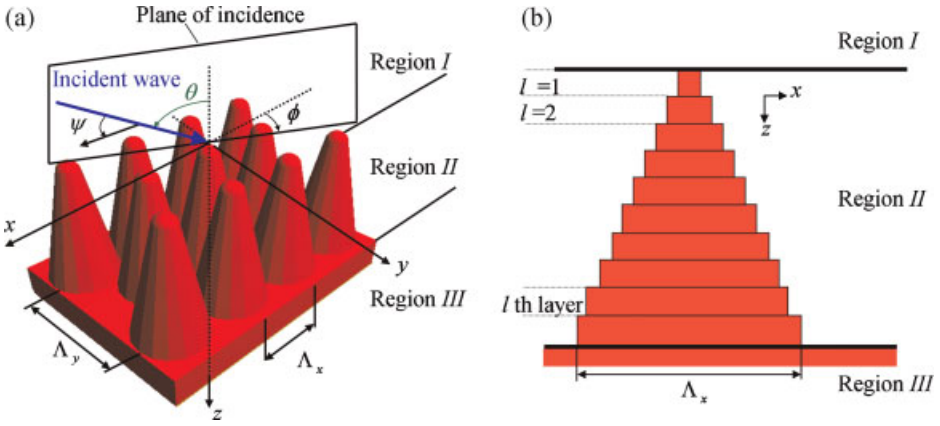


**Figure 2.** Geometrical structure of modeled moth-eye structure used for RCWA simulation. (a) Three-dimensional coordinate system. (b) Layered model in *x-z* plane.

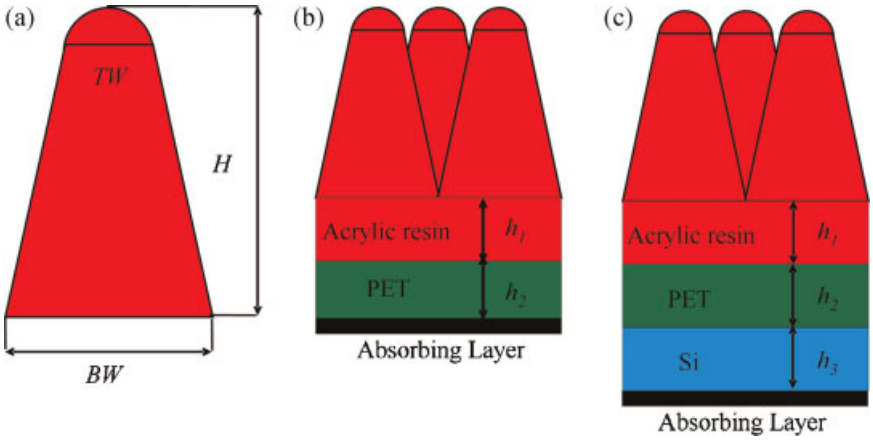


**Figure 3.** Simulation model of moth-eye structure. (a) Dimensions of nipple. (b) Model for reflectance calculation of moth-eye film. (c) Model for transmitted power calculation and shape optimization.

shape is optimized to maximize TP of the Si surface. Both the models have an absorbing layer that perfectly absorbs electromagnetic waves incident on its surface.

### 3.1. Reflectance characteristics of moth-eye structure

The reflectance of the structure is investigated in the wavelength range from 300 to 1600 nm. The following conditions are fixed in the simulation: $\Lambda_x = 100$ nm, $\Lambda_y = \sqrt{3}\Lambda_x$, $h_1 = 0.2$ mm, $h_2 = 0.037$ mm, $h_3 = 0.3$ mm, $\phi = 0^\circ$. The incident angle is set to $\theta = 5^\circ$, unless otherwise specified.

Figure 4 shows the reflectance of the moth-eye structure for $H = 100$–$500$ nm, $TW = 50$ nm, and $BW = 90$ nm. The reflectance is significantly reduced as the nipple height increases, especially in the infrared region. A low reflectance of less than 1% is observed over the entire spectral region of the simulation model when $H > 300$ nm.

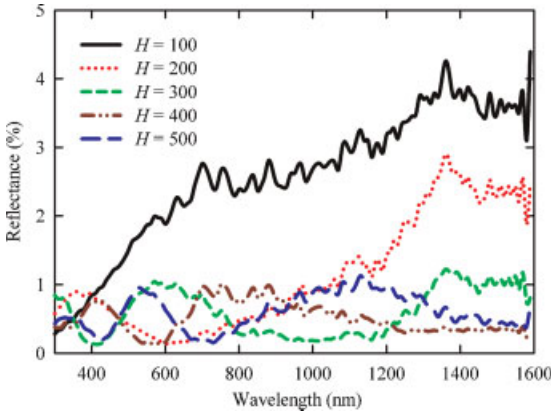


**Figure 4.** Reflectance of moth-eye structure for $TW = 50$ nm, $BW = 90$ nm, and $H = 100$–$500$ nm.


*Prog. Photovolt: Res. Appl.* 2011; **19**:134–140 © 2010 John Wiley & Sons, Ltd.
DOI: 10.1002/pip.994

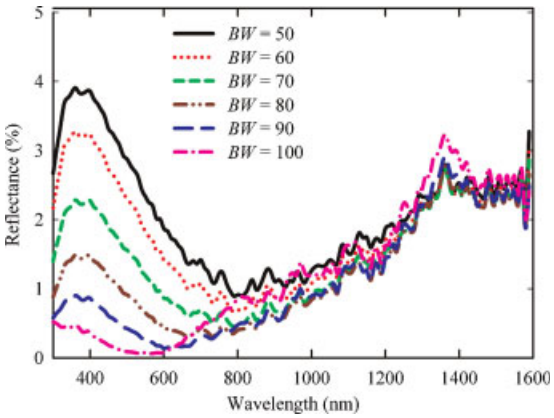


**Figure 5.** Reflectance of moth-eye structure for $TW = 50$ nm, $H = 200$ nm, and $BW = 50$–$100$ nm.

Figure 5 shows the reflectance of the moth-eye structure for $BW = 50$–$100$ nm, $TW = 50$ nm, and $H = 200$ nm. In the visible region, the reflectance is significantly reduced with an increase in $BW$. A minimum reflectance of 0.6% is observed at $BW = 100$ nm. In contrast, no significant differences are observed in the infrared region, i.e., above 800 nm.

Figure 6 shows the reflectance of the moth-eye film for $TW = 0$-$90$ nm, $BW = 90$ nm, and $H = 200$ nm. Two different tendencies are observed in the $TW$ range. Figure 6(a) shows the simulation result for $TW$ ranging from 0 to 40 nm; Figure 6(b) shows that for $TW$ ranging from 50 to 90 nm. When $TW < 40$ nm, reflectance decreases as $TW$ increases in the wavelength range. On the other hand, when $TW > 50$ nm, reflectance increases in the wavelength range from 300 to 700 nm, whereas no significant difference is observed in the wavelength range from 1000 to 1600 nm. At $TW = 50$ and 60 nm, a reflectance of less than 0.5% is observed in the wavelength range from 500 to 900 nm.

According to Baker [12], in order to achieve minimum reflectance and maximum transmittance using a micro-structure, the following conditions should be satisfied

- The nipple height must be at least 40% of the shortest operational wavelength ($\lambda$).

  $h = 0.4\lambda$
- The grating period must be less than the shortest operational wavelength divided by the refractive index of the material.

  $\Lambda < \lambda/n$
- When a substrate with a high refractive index (e.g., $n = 3.5$ for Si) is used, the refractive index must increase non-linearly. However, when glass or plastic ($n \approx 1.5$) is used, the refractive must increase linearly.

In the case of the structure used in this study, the condition of grating period is satisfied. The minimum reflectance should be achieved with $H > 200$ nm, $BW = 90$ or 100 nm, and $TW < 60$ nm. Each shape dimension has a specific wavelength of the minimum reflection in these conditions.

## 3.2. Shape optimization for maximizing transmitted power of c-Si cell surface

In this section, the moth-eye structure is optimized in order to achieve the maximum TP by the c-Si cell surface that is coated with the moth-eye film, as shown in Figure 3(c). The spectral response of the c-Si solar cell indicates that to achieve maximum TP, the nipple shape should be optimized in the wavelength range from 400 to 1170 nm. The following conditions are fixed: $h_1 = 0.2$ mm, $h_2 = 0.037$ mm, and $h_3 = 0.3$ mm. The Si surface is assumed to be flat, i.e., with no textural features such as random pyramids.

TP is defined as

$$TP = \frac{\int_{400nm}^{1170nm} SSI(\lambda) \times SR(\lambda) \times T(\lambda) \times d\lambda}{\int_{400nm}^{1170nm} SSI(\lambda) \times SR(\lambda) \times d\lambda} \quad (1)$$

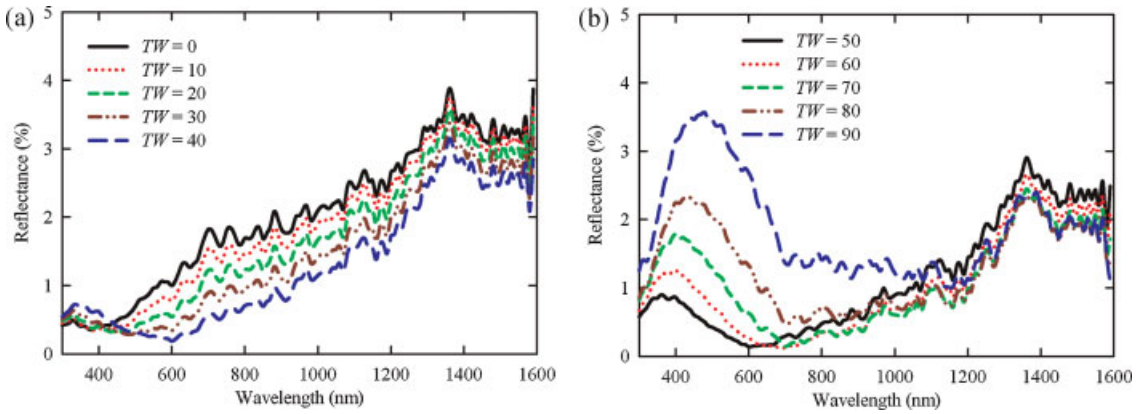


**Figure 6.** Reflectance of moth-eye film for $BW = 90$ nm, $H = 200$ nm, and (a) $TW = 0$–$40$ nm. (b) $TW = 50$–$90$ nm.

where SSI(λ) is the global solar spectral irradiance (W/m$^2$ $\mu$m) of standard AM1.5 solar spectrum [13], SR(λ)is the spectral response of the c-Si solar cell [14], and T(λ) is the transmittance of the moth-eye structure deposited on the Si surface. It is noted that ''transmittance'' denotes the ratio of the absolute transmitted energy to the total incident energy on the moth-eye structure. Low reflectance results in high transmittance when the thickness is constant.

In order to minimize the simulation trials for the optimization, Taguchi method [15] was used to identify the optimal values of three shape factors; $H$, $BW$, $TW$ to obtain the best TP. 14 values are selected as follows: $H=50$, 100, 200, 300, and 400 nm; $BW=60$, 70, 80, 90, and 100 nm; and $TW=0$, 30, 50, and 70 nm. A trial matrix with 23 combinations is formed, and TP is investigated for different combinations of these values. In the Taguchi method, the contribution of a certain parameter is evaluated by an index called ''average effect.'' For example, the average effect of $H=50$ nm is defined as the average simulated TP of the combinations that include the value $H=50$ nm.

The average effects are plotted in Figure 7. It is obvious that the optimum nipple shape is $H=300$ nm, $BW=100$ nm, and $TW=30$ nm. A TP of 83.91% is achieved. Hereafter, this optimized shape is referred to as an ''optimized moth-eye structure.''

Before carrying out the simulation, a moth-eye film with $H=200$ nm, $BW=90$ nm, and $TW=50$ nm is fabricated by a nanoimprinting technology using Ni molds, and it is used in the experiment, which is described later. Hereafter, this previously fabricated film is referred to as a ''fabricated moth-eye structure.'' An SEM image of the fabricated moth-eye structure is shown in Figure 1(b). The simulated TP of the fabricated moth-eye structure is 83.54%, i.e., 0.37% less than that of the optimized moth-eye structure. Figure 8 shows a comparison between the incident angle dependency of simulated TP of the optimized and fabricated moth-eye structures as compared with non moth-eye (i.e., flat acrylic resin) in the simulation model shown in Figure 3(c). The increase in TP is defined as

$$TP improvement = \frac{TP_{with moth-eye} - TP_{without moth-eye}}{TP_{without moth-eye}} \quad (2)$$

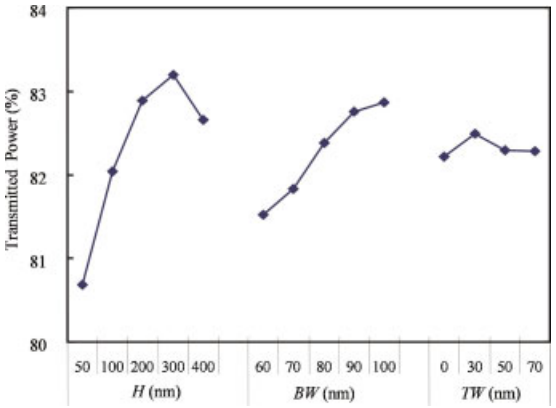


**Figure 7.** Average effects of *H*, *BW*, and *TW* on TP.

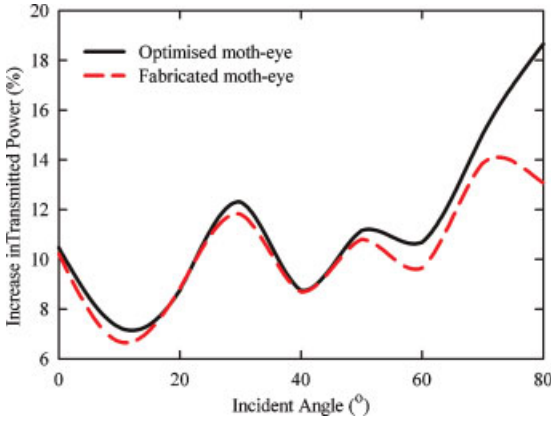


**Figure 8.** Comparison between incident angle dependency of simulated TP of optimized moth-eye structure ($H=300$ nm, $TW=30$ nm, and $BW=100$ nm) and fabricated moth-eye structure ($H=200$ nm, $TW=50$ nm, and $BW=90$ nm) as compared with non moth-eye in the simulation model shown in Figure 3(c).

The increase in TP of both the moth-eye structures varies from 7 to 12% when the incident angle $\theta<60°$. For $\theta>70°$, the increase in TP of the optimized moth-eye structure is approximately 5% larger than that of the fabricated one.

Figure 9 shows a comparison between the measured spectral reflectance of the fabricated moth-eye structure and the simulated reflectance of the fabricated and optimized moth-eye structures at $\theta=5°$ In the measurement, the backside of the fabricated moth-eye film is sandblasted and then coated with a matte-black paint to achieve the function of absorbing layer in the simulation model. In the simulation result of the fabricated moth-eye structure, a reflectance of less than approximately 1% is observed in the wavelength range from 400 to 1170 nm, and a minimal reflectance of 0.55% is observed at 700 nm although the shape is not optimized. The measured

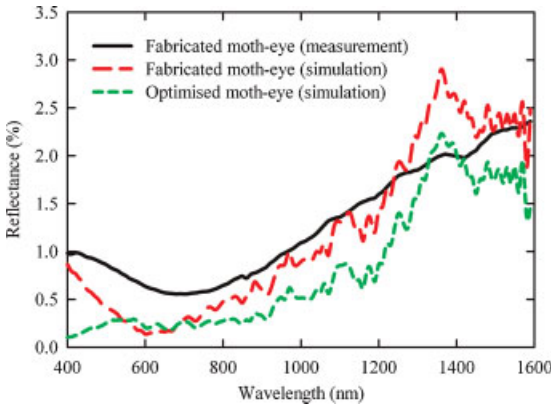


**Figure 9.** Comparison between measured reflectance of fabricated moth-eye structure and simulated reflectance of fabricated and optimized moth-eye structures at $\theta=5°$.


*Prog. Photovolt: Res. Appl.* 2011; **19**:134–140 © 2010 John Wiley & Sons, Ltd.
DOI: 10.1002/pip.994

reflectance tends to be slightly higher than the simulation result. This difference could be attributed to the difference in the nipple shape of the fabricated moth-eye structure and simulation model. On the other hand, the simulated reflectance of the optimized moth-eye is less than 0.87% in the wavelength range from 400 to 1170 nm, and a minimal reflectance of 0.1% is observed at 400 nm.

## 4. EXPERIMENTAL VERIFICATION

The effectiveness of the fabricated moth-eye film is evaluated by performing an experiment. A conventional c-Si solar cell with a planar surface area of $5.2 \times 6.8\,cm^2$ and cell efficiency of approximately 10% (absolute) without any AR coating is used, and TP with and without the fabricated moth-eye film is estimated. The c-Si cell without moth-eye film is encapsulated with flat PVB layer of uniform thickness with 0.5 mm. The cell system with the moth-eye film is as same as the simulation model shown in Figure 2(c), except that there is a PVB layer between PET and Si layer in the experimental cell system. In other words, the moth-eye film is just added on top of the PVB encapsulation layer of the cell system without moth-eye film. The incident angle dependency of EG for these configurations is elucidated by varying the incident angle from 0° to 80°.

The experiment is performed in January under actual sun light on clear and sunny days from 11:00 to 14:00 in Nagaoka, Japan. The incident global solar irradiance varies from 760 to 860 $W/m^2$ during the experiment. Samples are set on a tracking table. The incident angle is manually controlled using an angle adjuster. EG is measured using I-V measurement equipment; at the same time, the incident global solar irradiance is measured using a pyranometer. First, TP of the sample without a moth-eye film is measured. Then, a moth-eye film is deposited on the sample, and TP is measured again under the same solar irradiance. This procedure is repeated several times, and average values are obtained.

Figure 10 shows a comparison between the incident angle dependency of measured EG of the fabricated moth-eye structure and that of the simulated EG of the fabricated and optimized moth-eye structures as compared with the simulated TP improvements shown in Figure 8. Here, the increase in EG is defined as

$$EG\,improvement = \frac{EG_{with\,moth-eye} - EG_{without\,moth-eye}}{EG_{without\,moth-eye}} \quad (3)$$

The measured EG varies from 1.5% to over 15%, depending on the incident angle. On the other hand, the simulated TP varies from 6 to 18%. This difference is mainly caused by the mismatch between the experimental and simulation conditions. In the experiment, the c-Si cell is enclosed in a PVB layer; however, the PVB layer is not included in the simulation model. Without the PVB layer, an increase of approximately 6% is expected when the incident angle is less than 40°.

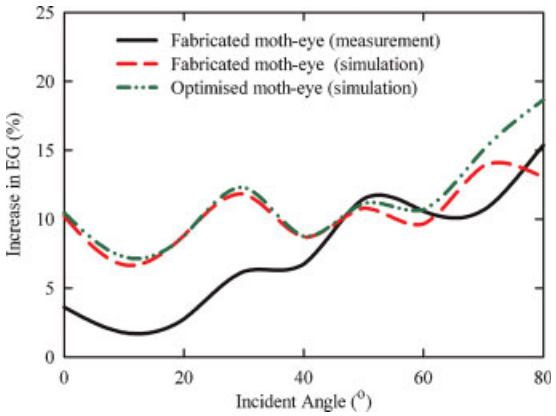


**Figure 10.** Comparison between incident angle dependency of measured EG of fabricated moth-eye structure and that of simulated EG of fabricated and optimized moth-eye structures as compared with the simulated TP improvements shown in Figure 8.

## 5. ESTIMATION OF DAILY INCREASE IN ELECTRIC GENERATION

Taking into account the incident angle dependency of measured EG, the daily increase in EG is estimated on a clear summer day in Tokyo (Longitude: 39°45′N, Lattitude: 35°40′E). Extended AMeDAS standard data, which are long-term average data acquired from 1981 to 1995, are used to obtain the beam and diffuse solar irradiance according to the position of the sun over Tokyo on 9th August. The diffuse irradiance is assumed to be isotropic. The PV module tilt angle is assumed to be 20°. The module is assumed to be facing south or east. The daily variation in the incident angle is calculated for both beam and diffuse irradiance with geometrical consideration; the daily increase in EG is then estimated by retrieving the data measured for the calculated incident angle.

Table I shows the estimated result of the daily increase in EG. It is expected to increase up to 8.7% using the optimized moth-eye structure and up to 6.7% using the fabricated moth-eye structure, with the module facing

**Table I.** Estimated daily increase in EG by coating conventional c-Si module with moth-eye film, at tilt angle of 20° on clear summer day in Tokyo.

| PV module direction | Fabricated moth-eye film (%) | Optimized moth-eye film (%) |
|---|---|---|
| South | 6.7 | 8.7 |
| East | 5.8 | 7.6 |

south. The increase in EG using the optimized moth-eye is expected be approximately 2% higher than that using the fabricated one.

## 6. CONCLUSIONS

In this study, the moth-eye structure made of acrylic resin and deposited on a PET substrate is optimized in the wavelength range from 400 to 1170 nm; c-Si solar cells function efficiently in this wavelength range. The optimized moth-eye nipple dimensions are as follows: 300 nm height, 100 nm bottom width, and 30 nm top width. The simulation results show that the reflectance of the optimized moth-eye structure is less than 0.87% in the above-mentioned wavelength range. The reflectance of the fabricated moth-eye structure—with dimensions of approximately 200 nm height, 90 nm bottom width, and 50 nm top width—is lower than approximately 1.0% in the above-mentioned wavelength range, and a minimal reflectance 0.55% is observed at 700 nm.

The conventional c-Si solar cell, which is enclosed in a PVB layer of uniform thickness, is coated with the fabricated moth-eye film, and it is elucidated that the film increases EG up to 15%, depending on the incident angle. Further, it is estimated that the daily increase in EG on a clear summer day in Japan is up to 6.7 and 8.7% in the case of the fabricated moth-eye structure and the optimized one, respectively. The authors expect the present moth-eye film can basically works when it is deposited on glass surface.

Moth-eye films with a surface area larger than that of the one used in this study can be fabricated by the existing technique. Ensuring reliability in case of long-term exposure is one of the major challenges.

## REFERENCES


1. Chopra K. *3rd Work Shop on Thin Films Physics and Technology Proceeding*. New Delhi, 1999; 8–24.
2. Bernhard CG. Structural and functional adaptation in a visual system. *Endeavour* 1967; **26**: 79–84.
3. Clapham PB, Hutley MC. Reduction of lens reflection by the moth-eye principle. *Nature* 1973; **244**: 281–282.
4. Stavenga DG, Foletti S, Palasantzas G, Arikawa K. Light on the motheye corneal nipple array of butterflies. *Proceeding Royal of Society B* 2006; **273**: 661–667.
5. Gombert A, Glaubitt W, Rose K, Dreibholz J. Subwavelength-structured anti-reflective surfaces on glass. *Thin Solid Films* 1999; **351**: 73–78.
6. Kaless A, Schulz U, Munzert P, Kaiser N. Nanomotheye antireflection pattern by plasma treatment of polymers. *Surface & Structures Technology* 2005; **200**: 58–561.
7. Yanagishita T, Yasui K, Kondo T, Kawamoto Y, Nishio K, Masuda H. Antireflection polymer surface using anodic porous alumina molds with tapered holes. *Chemistry Letters* 2007; **36**: 530–531.
8. Peng S, Morris GM. Efficient implementation of rigorous coupled-wave analysis for surface-relief gratings. *Journal of the Optical Society of America A* 1994; **12**: 1087–1096.
9. Moharam MG, Grann EB, Pommet DA. Formulation for stable and efficient implementation of the rigorous coupled-wave analysis of binary gratings. *Journal of the Optical Society of America A* 1995; **12**: 1068–1076.
10. Jarem JM, Banerjee PP. *Computational methods for electromagnetic and optical systems* 2000.
11. Moharam MG. Coupled-wave analysis of two-dimensional dielectric gratings. *SPIE* 1988; **883**: 8–11.
12. Baker KM. Highly corrected close-packed microlens arrays and moth-eye structuring on curved surfaces. *Applied Optics* 1999; **38**: 352–356.
13. Halden F. Solar cell spectral response measurement errors related to spectral band width and chopped light waveform *26th IEEE Photovoltaic Specialists Conference* 1997.
14. http://pvcdrom.pveducation.org/APPEND/Am1_5.htm. Date of access: 21 April 2009.
15. Roy R. *A primer on the Taguchi method* 1999.
16. Akasaka H. *et al.* Extended AMeDAS Weather data 2000.



DOI: 10.1002/pip.994